Amplitude effects allow short jetlags and large seasonal phase shifts in minimal clock models

Bharath Ananthasubramaniam[a], Christoph Schmal[b], Hanspeter Herzel[a]

[a]*Institute for Theoretical Biology, Charité Universitätsmedizin Berlin, 10115 Berlin, Germany*
[b]*Institute for Theoretical Biology, Humboldt Universität zu Berlin, 10115 Berlin, Germany*

Abstract

Mathematical models of varying complexity have helped shed light on different aspects of circadian clock function. In this work, we question whether minimal clock models (Goodwin models) are sufficient to reproduce essential phenotypes of the clock: a small phase response curve (PRC), fast jetlag and seasonal phase shifts. Instead of building a single best model, we take an approach where we study the properties of a set of models satisfying certain constraints; here a PRC to a one-hour pulse of three hours and clock periods between 22h and 26h. Surprisingly, almost all these randomly parameterized models showed a phase shift of about four hours between long and short days and jetlag durations of three to seven days in advance and delay. Moreover, intrinsic clock period influenced jetlag duration and entrainment amplitude and phase. Fast jetlag was realized in this model by means of a novel amplitude effect: the association between clock amplitude and clock period termed 'twist'. This twist allows amplitude changes to speed up and slow down clocks enabling faster shifts. These findings were robust to the addition of additional positive feedback to the model. In summary, the known design principles of rhythm generation – negative feedback, long delay and switch-like inhibition (we review these in detail) – are sufficient to reproduce the essential clock phenotypes. Furthermore, amplitudes play a role in determining clock properties and must be always considered, although they are difficult to measure.

Keywords: circadian clock; mathematical model; seasonality; twist; design principles

1. Introduction

Mathematical modeling in chronobiology has a long tradition [1–5]. In the last few decades, the underlying gene-regulatory networks were identified [6, 7] and subsequently, detailed kinetic models were designed [8–10]. Mathematical models helped study entrainment [11, 12], temperature compensation [13], mutant phenotypes [14, 15], jetlag [16, 17], and seasonality [18, 19]. Detailed kinetic models reach enormous complexity if multiple genes and feedbacks are included [15, 20–22].

In this paper, we step back and address the question whether or not simple models can reproduce phenotypic features, such as phase response curves (PRCs), entrainment, jetlag, and seasonality. We ask – what can we learn from a systematic analysis of generic models about the underlying mechanisms? How oscillator properties, such as period and amplitude, govern phenotypic features including jetlag and seasonality? We find that ensembles of quite basic models reproduce these phenotypic features surprisingly well. Moreover, it turns out that amplitudes have a strong effect on jetlag duration and entrainment phase.

As a starting point we summarize now major phenomenological features of circadian clocks: PRCs, jetlag, and seasonality. Then we introduce simple models of delayed negative feedback loops with switch-like inhibition.

1.1. Phase Response Curves (PRCs) characterize circadian oscillators

Pulses of light or other *Zeitgebers* can shift the phase of endogeneous oscillators allowing entrainment [23]. Advancing and delaying phase shifts are quantified traditionally by PRCs [2, 24, 25]. In mammals, even long-lasting bright light pulses induce phase-shifts of just a few hours [26–29]. We exploit these observations to parameterize our simple feedback models: the *Zeitgeber* strength in our models is adjusted to get a 3 hour difference between maximal delay and advance for 1h light pulses consistent with mouse data [27].

1.2. Short jetlags indicate flexibility of circadian clocks

Mammalian clocks are quite strong oscillators [30] and even 6.7h light pulses with 10000 lux can induce only phase shifts of a few hours [26]. Nevertheless, following shifts of day-night cycles by six hours (a common "jetlag protocol"), it is possible to reset the clock within a few days [31–34]. It has been shown previously [35] that global parameter optimization can reproduce small PRCs and short jetlags. Here, we study jetlag duration systematically in generic models without any prior parameter optimization.

1.3. Seasonality implies four hour shifts of entrainment phase

Most organisms adapt their intrinsic clock to seasonal variations of day length. In many cases the "midpoint of activity stays relatively stable" [36, 37]. Frequently, phase markers appear to be coupled to dusk or dawn [38]. A change from an 8:16 light-dark (LD) cycle to a 16:8 LD cycle implies phase shifts of about 4 hours. For example, midnight locked peaks are 4 hours after light offset in short (8h) nights, but 8 hours after offset in long (16h) nights. If morning and evening peaks follow dusk or dawn, their phases with respect to midnight have to be shifted by 4 hours between winter (8:16 LD) and summer (16:8 LD). Consequently, entrainment phase changes of about 4 hours allow sufficient seasonal flexibility.

1.4. Design of generic feedback models

A delayed negative feedback loop with switch-like inhibition is necessary to produce self-sustained oscillations. In the mammalian circadian clock, there are two feedback loops that feature these ingredients [21] (Figure 1A). First, *Bmal1* transcripts are translated to protein that activates *Rev-erba* transcription. *Rev-erba* after translation to protein inhibits *Bmal1* transcription, thus completing the loop. Second, *Per2* represses its own transcription after delays due to transcription, translation and nuclear import [39]. These two regulatory loops can be abstracted to the 'Goodwin' model (Figure 1B), where variables X, Y and Z are involved in a negative feedback loop. We use the Goodwin model, since it is a generic feedback model and can be easily extended to include other features, such as positive feedback (Figure 1C).

2. Results

2.1. A representative model reproduces clock features

We explored the behavior of models with the structure in Figure 1B, which is commonly called the 'Goodwin model'. We varied the six model parameters randomly within a predefined region in parameter space. Several model parameterizations (henceforth shortened to 'models') oscillated in a self-sustained manner (Figure 2A is a representative example). The *Zeitgeber* influences the model with an additive term to the production rate of state X. The *Zeitgeber* strength for each model was adjusted to get a three hour range for the phase response curve (PRC) to a one hour *Zeitgeber* pulse (Figure 2B); this served to normalize the entraining input across models. The 'Material and Methods' section contains a detailed description of the numerical simulations.

We characterized the seasonal phase shift and duration of jetlag for each model. The seasonal phase shift is the change in the phase of entrainment between short day (LD 8:16) and long day (LD 16:8). The

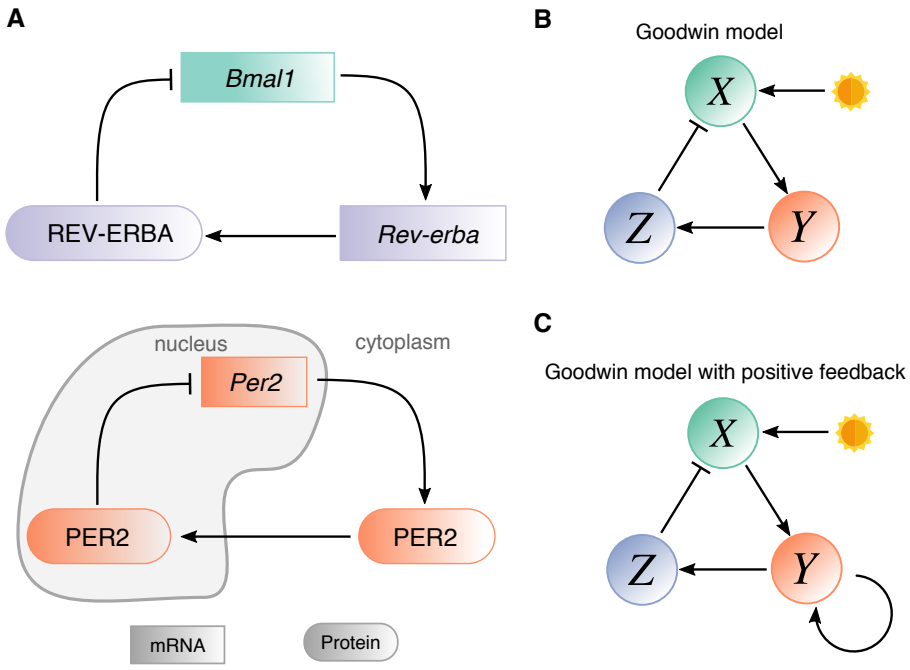

Figure 1: Schematic of minimal models. (A) Two possible gene-regulatory networks in mammalian circadian clock that can produce oscillations via a negative feedback. (B) The three variable model representing the schema in (A) with light input on variable X implemented in the simulations. (C) Variant of (B) with a positive feedback on variable Y.

seasonal phase shift of the model in Figure 2A is about four hours (Figure 2C). The phase of entrainment approximately tracks the midpoint of the dark phase.

We also subjected the models to advancing and delaying jetlag of six hours under a 24h (LD 12:12) *Zeitgeber* input (Figure 2D,E). An abrupt change in *Zeitgeber* phase (jetlag) shifts the phase of the model until a stable phase relative to the new *Zeitgeber* phase is achieved. The course of this change is the jetlag transient. The jetlag shifts simulated here represent flying from Berlin to New York (delay) or New York to Berlin (advance). The model shifted within 4-5 days to within 15 min of the final stable phase for both advancing and delaying jetlags. Moreover, the delaying jetlag shift was shorter than the advancing jetlag shift in this model.

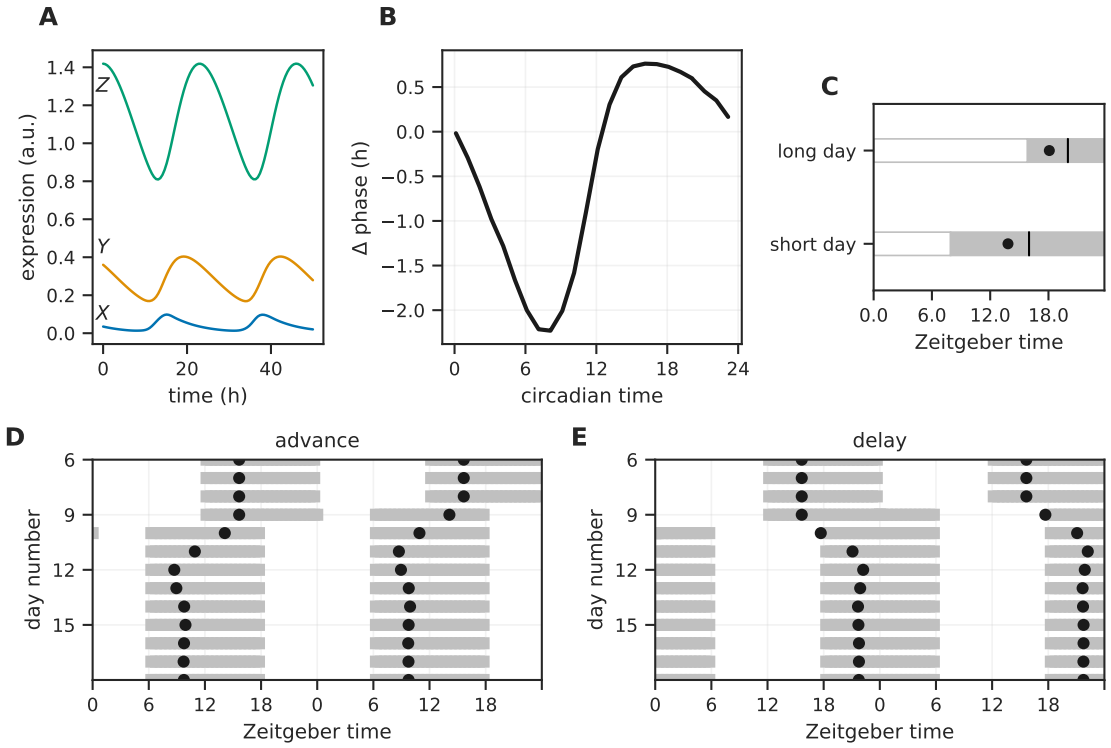

Figure 2: A representative model. (A) Time series of the three states (marked on the left) of the Goodwin model for a representative parameterization. (B) The phase response curve for the model in (A) in response to a one-hour pulse at different circadian times. (C) The phase of entrainment (black dots) measured relative to lights on under long day (LD 16:8) and short day (LD 8:16). The phase of entrainment is the acrophase of variable Z. (D, E) The acrophase of variable Z (black dots) during a 6h simulated jetlag from Berlin to New York (delay) or New York to Berlin (advance). Model Parameters: $d_1 = 0.15\text{h}^{-1}, d_2 = 0.15\text{h}^{-1}, d_3 = 0.25\text{h}^{-1}, K = 0.61, h = 11.44, \tau = 23.03\text{h}$.

2.2. *Short jetlag and large seasonal shifts are common*

The Monte Carlo approach outlined in the previous section generated an ensemble of models ($N = 1186$). All the models were self-sustained oscillators and had a PRC to a one-hour light pulse with a range of about three hours by design (Figure S1); we allowed a tolerance of 0.25h in order to speed up optimization of the *Zeitgeber* strength. We present here (Figure 3) the landscape of the duration of jetlag and magnitude of seasonal phase shifts within this ensemble.

The duration of the jetlag transient depends on the phase of the *Zeitgeber* at the instant of the jetlag shift in addition to the magnitude and direction of the jetlag shift. Therefore, jetlag was measured as the median jetlag duration starting at four phases 6h apart in order to capture the dependence on the starting phase. Since advancing and delaying jetlags were different (Figure 2), we present results for 6h advancing and 6h delaying jetlags separately.

The whole ensemble exhibited short jetlag shifts (about 3-7 days in length) and seasonal phase shifts of about four hours that matched the observed phenotypes described earlier. We expected specific optimized parameter sets alone to produce the necessary phenotypes [35]. Contrary to our expectation, randomly-chosen parameter sets with the same PRC yielded a highly clustered combination of reasonable jetlag duration and seasonal phase shift.

Advancing jetlag shifts were slower than delaying jetlag shifts (Figure 3). This might be anticipated from the larger delay region compared to a advance region in the PRC (Figure 2B). In fact, PRCs of all models in the ensemble had approximately a maximum advance of one hour and a maximum delay of two hours (Figure S1). We can roughly estimate (using the PRC) that an advance of one hour or delay of two

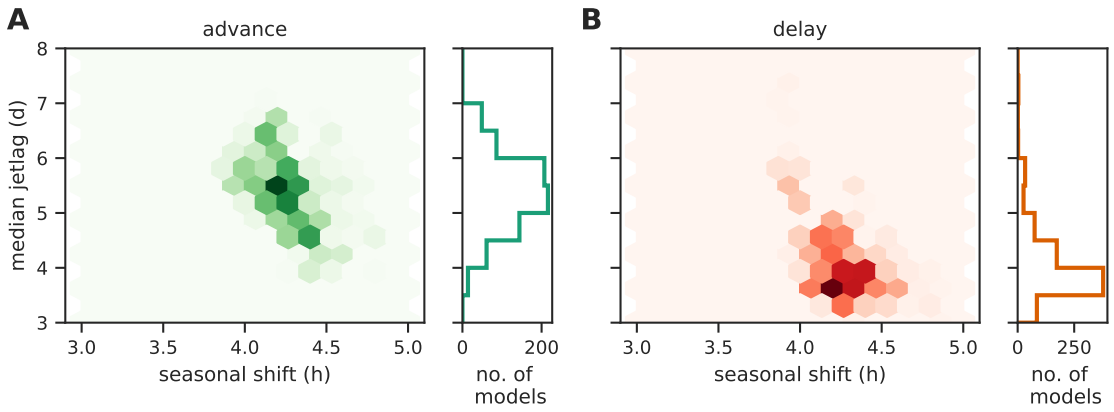

Figure 3: Landscape of jetlag duration and seasonal phase shifts. Combinations of median jetlag for a 6h advance (A) and a 6h delay (B) of the light-dark cycle and seasonal phase shift between long day (LD 16:8) and short day (LD 8:16) observed in the ensemble of models. The number of models for each combination of jetlag and seasonal shift are hexagonally-binned. The counts increase from the lightest to the darkest color.

hours requires a day. If shifts on subsequent days can be carefully adjusted, the simulated 6h jetlags would need six days for the advance or three days for the delay. Surprisingly, the randomly-parameterized models in the ensemble shifted as fast or sometimes faster than the rough estimates. We examine, in the remaining sections, the ensemble properties to better understand the mechanisms that result in the landscape in Figure 3.

2.3. Entrainment phases correlate with clock period

The theory of entrainment describes the relationship between the *Zeitgeber* strength, *Zeitgeber* period, intrinsic clock period and intrinsic clock amplitude in a certain clock (model) needed for entrainment. Entrainment has occurred once the clock achieves a fixed phase (called phase of entrainment ψ) with respect to the *Zeitgeber*. Instead of observing a single oscillator under a range of *Zeitgeber* periods, we observed the ensemble (comprised of models with different intrinsic clock periods) after entrainment to a 24h (LD 12:12) *Zeitgeber*. The heterogeneity of human circadian clocks was similarly used to study the entrainment properties of humans [40, 41].

Generally, short period clocks had earlier ψ and long period clocks had later ψ (Figure 4A). The slope of ψ versus clock period τ was small (slope ~ 0.5) across the ensemble. Unicellular organisms and plants under entrainment show such small slopes [42]. Moreover, entrainment theory predicts $\sim$12h change in the phase of entrainment across the entrainment range of an oscillator [2, 30]. This suggests a large entrainment range is necessary to achieve this small slope. We shall return to the range of entrainment in Figure 8.

The entrained amplitudes of the models in the ensemble, on the other hand, showed a small but significant decreasing trend with intrinsic clock period τ (Figures 4B-D); such an amplitude trend has been previously reported [43]. However, the intrinsic (unentrained) amplitude was uncorrelated with intrinsic clock period ($\rho = 0.03$, p-value=0.21). The observed trend arises from the phenomenon of 'twist' in these models; twist is an association between the amplitude and period of an oscillator. The representative model, for example, has a positive association between period and amplitude (Figure 6C). Therefore, when the *Zeitgeber* period is shorter than the intrinsic clock period, the entrained amplitude decreases (e.g., τ = 26h). The corresponding argument for shorter τ explains the decreasing trend in data. We will return to this amplitude effect in Figure 6.

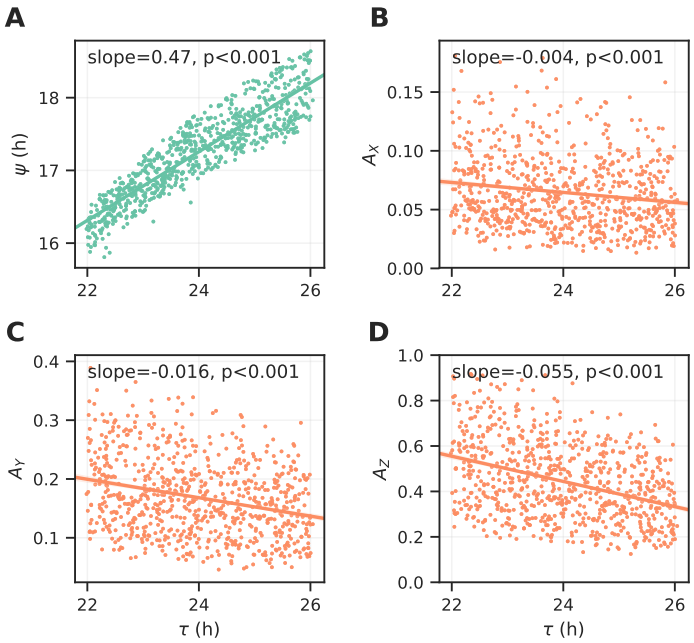

Figure 4: Entrainment properties of the ensemble of models. (A) Dependence of the phase of entrainment ψ to a 24h (LD 12:12) *Zeitgeber* on the intrinsic clock period τ of models in the ensemble. (B,C,D) Association between the entrained amplitudes of the three model variables X (B), Y (C), Z (D) and the intrinsic clock period of the models in the ensemble. A straight line regressed on the intrinsic period is also plotted.

2.4. Intrinsic periods affect length of jetlag

Both advancing and delaying jetlag were generally short throughout the ensemble. The PRC yielded reasonable rough estimates of jetlag duration. We could use the ensemble of models with their heterogeneous PRCs to test whether the PRC indeed can predict the jetlag duration. If this hypothesis were true, models with larger advance regions should have shorter advance jetlags and similarly models with larger delay regions should have a shorter delay jetlags. Models with larger delay regions (and smaller advance regions, since delay + advance region was chosen to be about three hours) indeed had shorter delay jetlag transients (Figure S3A). Intriguingly, models with larger delay regions (and smaller advance regions) also had shorter advance jetlag transients (Figure S3B). Therefore, the PRC alone is insufficient to describe the model's jetlag behavior. To gain further insight into the models, we explored the dependence of the duration of the jetlag on model parameter and properties.

Short intrinsic clock periods favor shorter advancing jetlags (ρ_{spearman} = 0.25, p-value $<$ 0.001, Figure 5A). Similarly, longer intrinsic periods favor shorter delaying jetlags, although the effect was less pronounced (ρ_{spearman} = -0.10, p-value = 0.008, Figure 5B). During an advancing jetlag transient, the entrained clock needs to speed up (reduce its period/increase its phase velocity) to achieve the new *Zeitgeber* phase. Thus, the shorter intrinsic period (faster clock) naturally aids the jetlag shift. Likewise, response to a delaying jetlag shift requires slowing the clock, which is favored in long intrinsic period clocks.

The Goodwin model requires a Hill coefficient of at least eight in order to oscillate. The Hill coefficient controls the degree of nonlinearity in the negative feedback loop, a necessary component of an oscillator. Models with stronger nonlinearity shifted faster in response to both advance (ρ_{spearman} = -0.56, p-value $<$ 0.001, Figure 5C) and delay jetlag shifts (ρ_{spearman} = -0.75, p-value $<$ 0.001, Figures 5D). The Goodwin model with higher Hill coefficients is associated with higher amplitude relaxation rates and faster entrainment (Figure S2) [44]. Amplitude relaxation rate measures the time taken for the effect of a perturbation

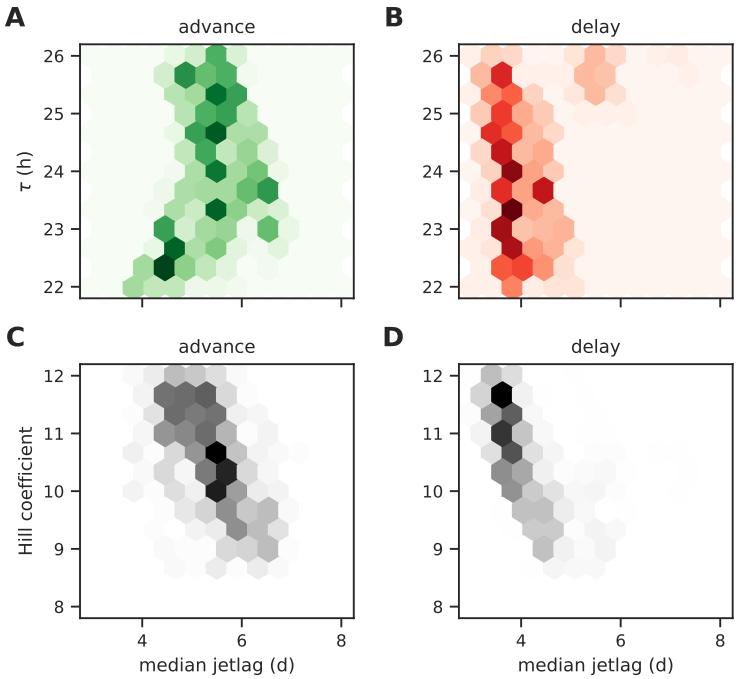

Figure 5: Dependence of jetlag on intrinsic clock period and model nonlinearity. (A, B) Variation of the duration of advance (A) and delay (B) jetlag for models with different intrinsic periods τ within the ensemble. (C, D) Influence of the degree of nonlinearity in the feedback loop (Hill coefficient) on the duration of advance (C) and delay (D) jetlags. The number of models for each combination of jetlag and model parameter are hexagonally-binned. The counts increase from the lightest to the darkest color.

to disappear [12, 44]. We suspect the faster time to entrainment is closely related to the duration of jetlag transient.

2.5. Amplitude changes facilitate short jetlag

We earlier observed that both the amplitude and the jetlag duration varied with the instrinsic clock period (Figures 4 and 5). We wondered whether the amplitude of the oscillator played a role in aiding the short jetlags. Therefore, we observed the behavior of the representative model from Figure 2 during simulated advancing and delaying jetlags.

The amplitude of the clock changed significantly over the course of the jetlag transient (Figure 6). The clock amplitude decreased from the steady-state entrained amplitude during a 6h advance (Figure 6A), but returned to the amplitude prior to jetlag after the phase shift had been achieved. On the other hand, the clock amplitudes increased relative to the steady-state amplitudes during a 6h delay. This leads one to question how these amplitude changes aid in shifting the clock phase during jetlag.

To this end, we characterized the *twist* or amplitude-period association of this model without *Zeitgeber* input. We observed how the amplitude and period of the clock varied near the steady-state rhythm (*limit cycle*). The instantaneous amplitude and period of the clock as the perturbed (unentrained) clock returns to the limit cycle is used to measure twist (Figure 6C). It is clear that there is an approximately linear relationship between amplitude and period. Smaller periods are associated with smaller amplitudes and larger periods with larger amplitudes. When the clock phase needs to be advanced, during a jetlag advance, a reduced amplitude is accompanied by a faster clock (i.e., smaller period), which facilitates the advance. Similarly, during a jetlag delay, where phase needs to be delayed, an increased amplitude coincides with a slower clock (i.e., larger period) that aids the delay. This interpretation is consistent with amplitude changes seen in Figures 6A,B.

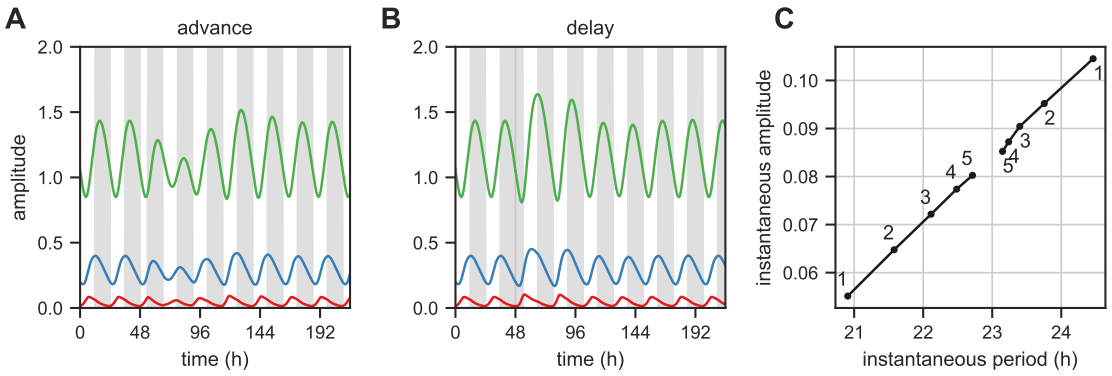

Figure 6: Amplitude changes during jetlag facilitate the phase shift. (A, B) Time series of the representative model in Figure 2 during a 6h jeltag advance (A) and a 6h jetlag delay (B). The dark period of the light-dark cycle is colored grey. Jetlag occurs at $t = 48$h. (C) A measure of the twist (amplitude-period association) of the representative model. The instantaneous amplitude and period of the model as it returns to the unperturbed state after a perturbation of $\epsilon = 0.1$ in two opposite directions (the sequence of amplitude and period values is numbered. Only the first five points are shown). Amplitude of variable X is used as the amplitude measure.

The amplitude of even the minimal models used here is difficult to define uniquely. The amplitude of each variable in the model can be measured, but it is unclear how these amplitudes can be reduced to a single metric for the whole model. Fortunately, consistent changes in amplitude occur across all three model variables during jetlag and the definition of amplitude does not affect our conclusions.

2.6. Observations are robust to addition of positive feedback

We have previously observed that many negative feedback oscillators have auxiliary positive feedback loops [39]. Moreover, the core clock network does include many positive feedback loops in the form of Michaelis-Menten (MM) degradation, complex formation and nuclear import-export. We therefore investigated the effect of a positive feedback in the form of MM degradation of variable Y on our observations.

A representative model with positive feedback oscillates (Figure S4A) and has a PRC with about an one hour advance and a two hour delay (Figure S4B), similar to the Goodwin model. The transient after a 6h phase advance or 6h phase delay lasts about four to six days (Figure S4D,E) and the seasonal phase shift between long and short day is also around four hours (Figure S4C).

At the ensemble level, the landscape of jetlag duration and seasonal phase shift (Figure 7A) was tightly clustered like the landscape of the Goodwin model (Figure 3). However, the jetlag duration for both delay and advance was slightly longer with positive feedback. Delay jetlag remained shorter than advance jetlag even with positive feedback. The seasonal phase shift was also consistently shorter by about 0.5h with positive feedback. Nevertheless, the qualitative features of short jetlag and seasonal phase shift was robust to these model changes.

The phase of entrainment ψ varied by almost the same slope with positive feedback (Figure 7B). This suggests that the entrainment properties of the model are conserved. When we examined the dependence of short jetlag on the model parameters, the jetlag duration was very weakly affected by intrinsic clock period (Figure 7C). The advancing jetlag transients were unaffected by the circadian period (ρ_{spearman} = -0.05, p-value = 0.18), while delaying jetlag transients possessed a weaker reversed trend with respect to instrinsic clock period (ρ_{spearman} = 0.11, p-value = 0.002). Higher Hill coefficients consistently favored shorter jetlag duration for both advance (ρ_{spearman} = -0.54, p-value < 0.001) and delay (ρ_{spearman} = -0.52, p-value < 0.001, Figure 7D). Positive feedback allows oscillations even for smaller Hill coefficients (below eight) [45], which can be seen from the greater spread of Hill coefficients in the ensemble. Furthermore, short jetlag was obtained consistently along a range of Hill coefficients.

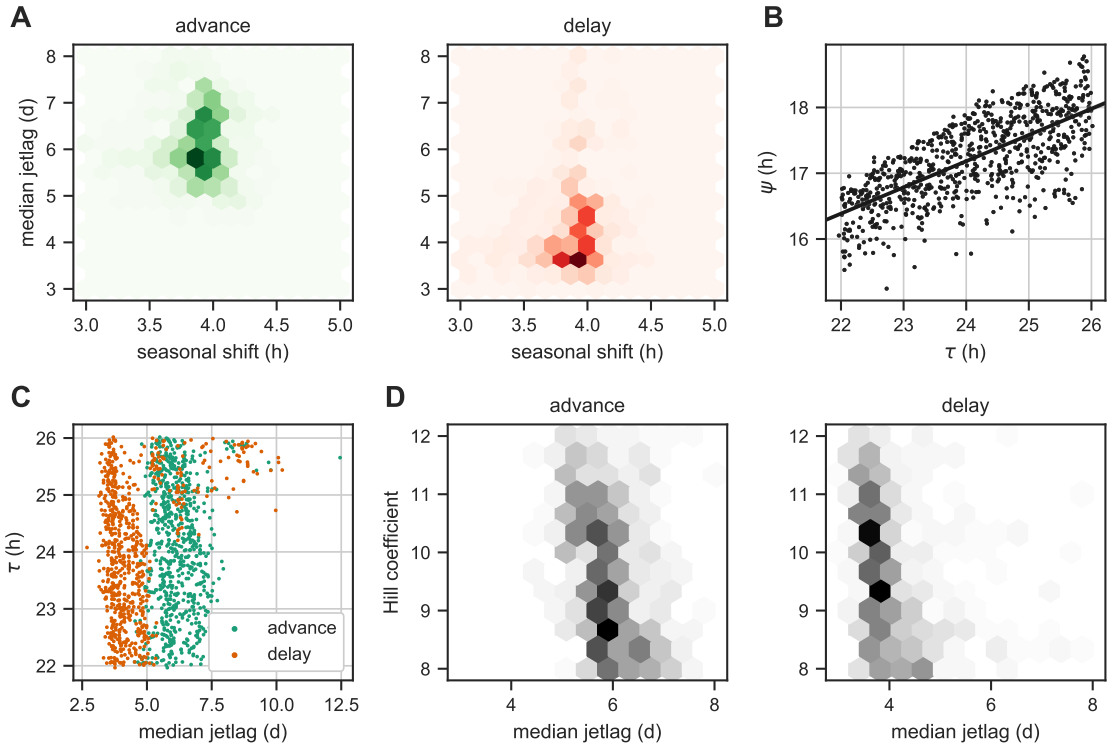

Figure 7: Model phenotypes with an auxiliary positive feedback loop. (A) The landscape of the median jetlag in response to a 6h shift and seasonal phase shift between long day (LD 16:8) and short day (LD 8:16); compare with Figure 3. The advancing (left) and delaying (right) jetlags are shown separately. (B) Dependence of the phase of entrainment ψ to a 24h (LD 12:12) *Zeitgeber* on the intrinsic clock period of models in the ensemble; compare with Figure 4A. (C) Variation of the duration of advancing and delaying jetlag (A) for models with different intrinsic periods within the ensemble; compare with Figures 5A,B. (D) Influence of the degree of nonlinearity in the feedback loop (Hill coefficient) on the duration of advance and delay jetlags; compare with Figure 5C,D. The number of models for each combination of parameters in (A) and (D) are hexagonally-binned. The counts increase from the lightest to the darkest color.

Amplitude changes were also observed in the representative model with positive feedback (Figure S4F,G). As with the Goodwin model, jetlag phase advances were accompanied by amplitude reduction and jetlag phase delay by amplitude expansion. This favors short jetlag transients, since the model even with positive feedback has a positive amplitude-period association or *twist* (Figure S4H) [46]. This allows speeding up the clock with amplitude reduction and slowing down the clock with amplitude expansion that can be used to efficiently overcome jetlag.

3. Discussion

Circadian rhythms are self-sustained oscillations that can be entrained by light-dark cycles. Mathematical models of these rhythms exhibit limit cycles driven by pulses or periodic inputs from a *Zeitgeber*. Any useful model should reproduce known basic phenotypic features, such as the PRC, phase of entrainment and jetlag duration.

In our paper, we studied ensembles of generic feedback models to explore systematically oscillator properties that allow short jetlags and large seasonal phase shifts. These generic models are minimal and contain just six parameters. The *Zeitgeber* strength was adjusted to get a PRC with a range of three hours for a one-hour light pulse [27]. The remaining parameters were randomly sampled in reasonable ranges. Models exhibiting self-sustained oscillations with an intrinsic period between 22h and 26h were analyzed in

detail. The resulting set of hundreds of models could be exploited to study connections between oscillator properties and phenotypic features.

Figure 2 demonstrates that a minimal model with a reasonable PRC has large seasonal flexibility and short jetlags. We show in Figure 3 that these features are reproduced by the whole ensemble of models. Furthermore, we analyzed how periods, amplitudes and entrainment phases are related (Figure 4) and studied dependencies of jetlag duration on intrinsic periods and strengths of nonlinearities (Figure 5).

Figure 6 illustrates an interesting mechanism: amplitude changes can affect jetlag duration. It has been described earlier in experimental studies that small amplitude oscillators are easy to reset [12, 47–50]. In these examples mutations and compromised coupling improved resetting and shortened jetlag. In Figure 6C, we point to another amplitude effect: correlations of amplitudes and periods (termed "twist") imply that *Zeitgeber*-induced amplitude changes can speed up or slow down oscillations. Consequently, transient amplitude changes as shown in Figures 6 and S4 can tune jetlag duration.

In order to evaluate the robustness of our result, we generated another ensemble of models with an auxiliary positive feedback. Figures 7 and S4 demonstrated that parameter dependencies and reproduced features do not change drastically.

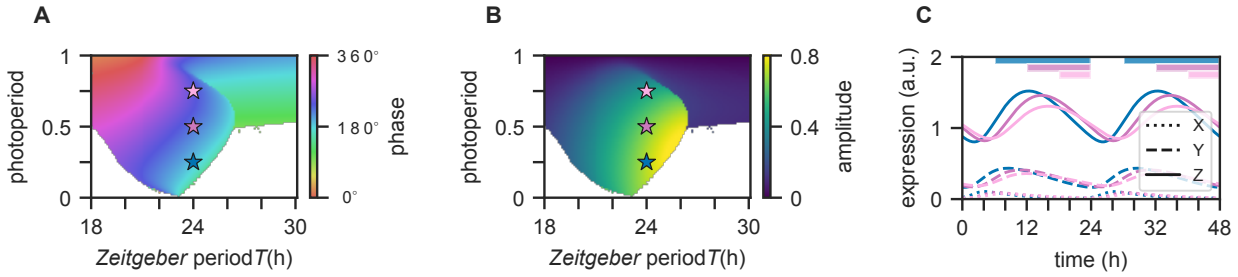

Figure 8: Entrainment properties of the representative model (Figure 2) under varying photoperiods and *Zeitgeber* periods. (A) Entrainment region of the clock model for different *Zeitgeber* periods T and photoperiods. Entrainment phases of variable Z are color-coded, while regions where no entrainment occurs are depicted by white color. Here, phases (in degrees) are defined as the acrophase of variable Z with respect to dawn (lights-on) normalized to the *Zeitgeber* period T. (B) Color-coded oscillation amplitudes of the variable Z within the entrainment region. (C) Exemplary simulations of the X (dotted lines), Y (dashed lines), Z (bold lines) variables in case of LD 8:16 (blue), LD 12:12 (purple), LD 16:8 (pink) entrainment under a $T = 24$h *Zeitgeber* period. Colored bars denote periods of darkness. *Zeitgeber* period and photoperiod combinations have been highlighted by correspondingly colored stars in panels (A) and (B).

Many of the described results can be quantified by extensive bifurcation analysis of the models [19]. Figure 8 shows an example of a two-dimensional bifurcation diagram for the representative model: the entrainment range, phase (Figure 8A) and amplitude (Figure 8B) are presented for varying *Zeitgeber* period and photoperiod. It turns out that entrainment phases and amplitudes vary widely. Selected model timecourses (Figure 8C) demonstrate again that amplitudes and entrainment phases co-vary.

Another interesting observation is the abrupt widening of the entrainment range for long days. Bifurcation analysis (Figure S5) reveals that this finding results from systematic changes due to increased light on long days. As found previously in another model [19, 51], increasing input can transform self-sustained oscillations to damped oscillations (a reverse "Hopf bifurcation"). Damped oscillations can be driven by any extrinsic periodic force and hence the "entrainment range" is huge. However, the amplitudes decrease drastically for large *Zeitgeber* periods (Figure 8B).

In the following sections, we discuss general aspects of mathematical models of circadian clocks. We emphasize that models are useful on different levels, that long days and switches are necessary for self-sustained oscillations, and that amplitudes are quite important to understand jetlag duration and seasonal flexibility.

3.1. Modeling can be applied on different levels

We analyzed generic models of a negative feedback loop. The required delay was achieved by a chain of reactions and slow degradation rates. The switch-like inhibition was modeled by a high Hill coefficient. Such a Goodwin model was motivated by self-inhibition of the Period and Cryptochrome genes and the *Bmal1-Rev-erba* loop. However, in contrast to previous models [15, 22, 52, 53], we did not fit the models to specific expression data. This implies that our models, while not quantitative in detail, can nevertheless be applicable in a wider context including in organisms other than mammals.

We emphasize that mathematical models of circadian rhythms can be applied on the single cell level describing gene-regulatory feedback loops. Other models might be appropiate on the tissue level, or on the organismic level. The available experimental data are quite heterogeneous. On the genetic level, the phenotypes of many mutants and downregulations are available [54, 55]. On the organ level, many expression profiles have been measured [56, 57]. On the organismic level many data on periods, entrainment phases and PRCs are documented [24, 42]. Consequently, also a great diversity of mathematical models have been developed including phenomenological amplitude-phase models [58], oscillator networks [51], explicit delay models [52, 59] and detailed kinetic gene regulation models [60]. Complex models can reproduce multiple mutants [20, 21] and pharmacological interventions [60].

Here we studied basic Goodwin models [61] that reproduced PRCs, jetlag, and seasonal adaptation surprisingly well. It has been shown earlier that mechanisms of temperature compensation could be also addressed with a simple Goodwin model [13]. Such generic models focus on the most important features of self-sustained oscillations: delayed negative feedback loops and switch-like inhibition.

3.2. Circadian rhythm generation requires a 6 hour delay

Under quite general conditions mathematical theory predicts that self-sustained oscillations with a period of 24 hours require a delay of at least 6 hours [52, 62, 63]. Most transcriptional-translational feedback loops introduce delays of about an hour and thus the corresponding periods are in the range of a few hours [64–66]. In order to reach periods of 24 hours, specific extra delays are required. In *Drosophila*, nuclear import of PER and TIM proteins is delayed by about six hours [67]. In mammals and *Neurospora crassa* multiple phosphorylations of the intrinsically disordered proteins PER2 and FRQ contribute to long delays [68–71]. Furthermore, cytoplasmatic and nuclear complex formation [72] and epigenetic regulations [73] can induce delays.

3.3. Possible mechanisms of switch-like inhibition

In our simple models, a high Hill coefficient is needed to get self-sustained oscillations [45]. Extended models have more realistic exponents due to longer reaction chains [74], positive feedback [39], protein sequestration [75] and protein inactivation [76]. In any case, switch-like inhibitions are required to get self-sustained rhythms. Theoretical studies have shown that switches can be obtained by cooperativity [77, 78], positive feedbacks [79], competition of antagonistic enzymes [80], and by sequestration [81]. In mammalian clocks, the most essential nonlinearities ("switches") are not precisely known. It is likely, that multiple phosphorylations [82], complex formations [72], and nuclear translocation [69] play a role. Presumably, the competition of histone acetylation and deacetylation plays an important role since several HATs and HDACs influence clock properties [83]. Moreover, histone modifications are modulated by PER and CRY binding [72]. Similar cellular mechanisms have been described in the *Neurospora* clock [84].

4. Conclusions

Our model simulations show that amplitudes have pronounced effects on jetlag duration and entrainment phase. Typically, periods are the main focus of chronobiological studies since there are established devices,

such as running wheels or race tubes, to measure periods. The measurement of amplitudes is less straight forward. Quantification of activity records [85] or conidation in race tubes [86] reflects just specific outputs. Gene expression profiles have to be carefully normalized for amplitude quantification [52]. Furthermore it is not immediately evident which gene is representative of the core clock amplitude. In *Neurospora*, FRQ and WCC amplitudes have been considered [87, 88]. In mammals, PER2 [89] and *Rev-erba* levels [90] have been used to quantify amplitudes. Measuring the response to pulses provides an indirect quantification of limit cycle amplitudes [89, 91, 92]. Small amplitude limit cycles exhibit larger pulse induced phase shifts than large amplitude limit cycles [25]. Despite the complexities in quantifying amplitude, we suggest studies take into consideration amplitude in addition to the standard phase-based metrics, such PRCs.

Our comprehensive analysis of generic feedback oscillators provides insight into the design principles of circadian clocks. The essential role of fine-tuned delays and molecular switches is emphasized by mathematical modeling. Reasonable jetlag durations and remarkably large seasonal variations of the entrainment phase can be reproduced by quite simple models. Our models stress the important role of circadian amplitudes. Simulations show that amplitudes contribute significantly to phenotypic features such as jetlag duration and seasonal adaptation.

5. Acknowledgements

B. A., C. S. and H. H. acknowledge support from the Deutsche Forschungsgemeinschaft (DFG) (SPP 2041, HE2168/11-1, TRR 186-A16). In addition, C. S. acknowledges support from DFG (SCH3362/2-1).

6. Material and Methods

6.1. Model structure – Goodwin model

We chose the Goodwin model to represent the core circadian clock feedback loop like many earlier works [13, 51, 93] (Figure 1B). Theoretically, the three variables in this model are the minimum number required to produce self-sustained oscillations. We further reduced the number of parameters in the standard model by using the fact that amplitudes can be rescaled; this is often called nondimensionalization. This yielded a model with five parameters (d_1, d_2, d_3, K, h):

$$\begin{aligned} \frac{dX}{dt} &= \frac{1}{1+\left(\frac{Z}{K}\right)^h} - d_1 X \\ \frac{dY}{dt} &= X - d_2 Y \\ \frac{dZ}{dt} &= Y - d_3 Z. \end{aligned} \tag{1}$$

d_1, d_2 and d_3 are degradation parameters with units h^{-1}. h is the Hill coefficient (unitless) that controls the strength of the nonlinearity in the loop and K is the half-maximum concentration of the Hill function controlling the repression of X by Z.

If the model oscillates for a particular choice of parameters, the period of oscillation τ' is some complex function of the parameters. Scaling the equations produces a model with a desired period of oscillation τ:

$$\begin{aligned} \frac{dX}{dt} &= \frac{\tau'}{\tau}\left(\frac{1}{1+\left(\frac{Z}{K}\right)^h} - d_1 X\right) \\ \frac{dY}{dt} &= \frac{\tau'}{\tau}\left(X - d_2 Y\right) \\ \frac{dZ}{dt} &= \frac{\tau'}{\tau}\left(Y - d_3 Z\right). \end{aligned} \tag{2}$$

Finally, the input to the clock from the *Zeitgeber* was modeled as an addition to the rate of production of variable X. The *Zeitgeber* input consisted of the *Zeitgeber* strength L times $I(t)$, where $I(t) = 1$ during the day (light phase) and $I(t) = 0$ during the night (dark phase). The model used for studying entrainment, jetlag simulation and seasonal phase shift was:

$$\begin{aligned} \frac{dX}{dt} &= \frac{\tau'}{\tau}\left(\frac{1}{1+\left(\frac{Z}{K}\right)^h} - d_1 X\right) + L\, I(t) \\ \frac{dY}{dt} &= \frac{\tau'}{\tau}\left(X - d_2 Y\right) \\ \frac{dZ}{dt} &= \frac{\tau'}{\tau}\left(Y - d_3 Z\right). \end{aligned} \tag{3}$$

6.2. Monte Carlo simulations

In order to study the generic behavior of the Goodwin model, we resorted to the Monte Carlo approach. In this approach, model parameters are chosen randomly to obtain an ensemble of models that can be studied for a variety of phenotypes. We now outline the schema of our simulations.

We randomly generated values for the five model parameters. In addition, we also chose a random intrinsic clock period for each model in order to have a uniform distribution of intrinsic periods in the ensemble. In this manner, 2000 different sets of six parameters were generated using latin hypercube sampling (LHS). LHS ensures that parameter sets explore the entire chosen range of each parameter. The degradation parameters could vary between 0.1 and 0.3 to get oscillation periods around 24h. The Hill coefficient could lie between five and twelve. The Goodwin model requires a Hill coefficient of at least eight [45], but the model with positive feedback can oscillate also with smaller Hill coefficients [39]. The half-maximum concentration of the Hill term was chosen between 0.25 and 1 in line with common values taken by the variable Z (see (2)). Finally, the instrinsic period was restricted to 22h to 26h based on the range of periods seen in mammalian clocks.

For each random choice of parameter values, we tested whether the model oscillated robustly. If it did, then we optimized the *Zeitgeber* strength L such that the PRC to a one hour pulse had a maximum phase range (largest advance - largest delay) of 3 ± 0.25h. Bear in mind that scaling the model to reduce parameters makes the oscillator amplitudes arbitrary. The entrainment behavior of the model depends on the ratio between the *Zeitgeber* strength and the oscillator amplitude. We used the constraint on the PRC to keep effect of the *Zeitgeber* consistent across models in the ensemble.

With the optimized *Zeitgeber* strength L^*, we ensured that the model can entrain to a 24h (LD 12:12) *Zeitgeber*. Upon entrainment, the phase of entrainment ψ is computed as the acrophase of variable Z relative to the lights-on (0 to L transition) of the *Zeitgeber*. Only when the model oscillates and is entrainable, we computed phenotypes of the model.

For each model, the seasonal phase shift is the difference between the phase of entrainment ψ for long day (24h LD 16:8 *Zeitgeber*) and short day (24h LD 8:16 *Zeitgeber*). Furthermore, for each model, we simulated jetlags with both a 6h phase advance and a 6h phase delay. This ensured also that our comparisons are well defined and data for advance and delay are always paired. Since the jetlag duration depends on the *Zeitgeber* phase when the phase shift occurs, we computed the median of the jetlag durations for 6h shifts starting from four different initial *Zeitgeber* phases (0, 6h, 12h, 18h). We measured jetlag duration from time of the *Zeitgeber* shift to the time point after which the phase of entrainment ψ of the clock stayed within 15 min of the final (shifted) phase.

6.3. Addition of positive feedback

We have previously defined the basic Goodwin model with different possible auxiliary positive feedback loops [39] and their significance in the mammalian circadian clock. Here, we used a variation of Goodwin

model with Michaelis-Menten (MM) degradation of the variable Y (Figure 1C):

$$\begin{aligned} \frac{dX}{dt} &= \frac{\tau'}{\tau}\left(\frac{1}{1+\left(\frac{Z}{K}\right)^h} - d_1 X\right) + L\, I(t) \\ \frac{dY}{dt} &= \frac{\tau'}{\tau}\left(X - \frac{d_2 Y}{1+cY}\right) \\ \frac{dZ}{dt} &= \frac{\tau'}{\tau}\left(Y - d_3 Z\right), \end{aligned} \tag{4}$$

where c controls the strength of the positive feedback. In reality, for each simulated standard Goodwin model, we computed the phenotypes for the related positive feedback model (4) by randomly choosing a c value between 0.5 and 5. Thus, the comparisons between standard Goodwin and Goodwin with positive feedback models are well-defined, since parameter sets/models are paired. In practice, LHS generated sets of seven variables (five model parameters + instrinsic period + positive feedback strength) and these values were used to simulate the Goodwin model and the corresponding positive feedback model. The computation of model phenotypes was exactly as previously described.

6.4. Arnold Onion

The Arnold Onion visualizes the entrainment behavior of the representative Goodwin model (Figure 2) for different combinations of *Zeitgeber* period and photoperiod. For each combination of *Zeitgeber* period T and photoperiod, we numerically solved (2) for a total integration time of 2020 entrainment cycles T at a step size of $\Delta t = 0.01$h. Transient dynamics within the first 2000 cycles were neglected. Next, we saved the complete state of the system at the beginning of the 2001st entrainment cycle and determined whether the system returns to the close neighborhood of this state, given by an ϵ-ball of radius 0.01 as described in [19]. Stable recurrence times equal to the *Zeitgeber* period T suggests an entrained state of the Goodwin oscillator. This is cross-validated by demanding a minimal of oscillation peak values of the Z variable. Phases within the entrained region were determined as a the distance between dawn, i.e., lights-on, and the peak time of the oscillations of the Z variable. Amplitudes are determined as half of the difference between the peak and trough values.

6.5. Floquet Multipiers

The speed at which the model returns to the limit cycle after a perturbation is measured by the amplitude relaxation rate. The average relaxation rate over one cycle can be calculated using the continuation software AUTO07p [94]. The software computes the so-called Floquet multipliers for any model defined using ordinary differential equations. These multipliers then are related to the amplitude relaxation rate.

6.6. Bifurcation Analysis

The bifurcation analysis of the model in Figure 2 was performed using XPPAUT with a constant *Zeitgeber* input, whose intensity was varied (Figure S5). Our approach is outlined in [95].

7. References

References

[1] K. Klotter, Theoretical analysis of some biological models, Cold Spring Harbor Symposia on Quantitative Biology 25 (0) (1960) 189–196. doi:10.1101/SQB.1960.025.01.017.

[2] R. Wever, Zum Mechanismus der biologischen 24-Stunden-Periodik: III. Mitteilung Anwendung der Modell-Gleichung, Kybernetik 2 (3) (1964) 127–144. doi:10.1007/BF00306797.

[3] A. T. Winfree, Biological rhythms and the behavior of populations of coupled oscillators, Journal of Theoretical Biology 16 (1) (1967) 15–42. doi:10.1016/0022-5193(67)90051-3.

[4] T. Pavlidis, Populations of interacting oscillators and circadian rhythms, Journal of Theoretical Biology 22 (3) (1969) 418–436. doi:10.1016/0022-5193(69)90014-9.

[5] S. Daan, C. Berde, Two coupled oscillators: Simulations of the circadian pacemaker in mammalian activity rhythms, Journal of Theoretical Biology 70 (3) (1978) 297–313. doi:10.1016/0022-5193(78)90378-8.

[6] P. E. Hardin, J. C. Hall, M. Rosbash, Feedback of the Drosophila period gene product on circadian cycling of its messenger RNA levels, Nature 343 (6258) (1990) 536–540. doi:10.1038/343536a0.

[7] H. Ukai, H. R. Ueda, Systems biology of mammalian circadian clocks, Annual Review of Physiology 72 (1) (2010) 579–603. doi:10.1146/annurev-physiol-073109-130051.

[8] D. B. Forger, C. S. Peskin, A detailed predictive model of the mammalian circadian clock, Proceedings of the National Academy of Sciences U.S.A. 100 (25) (2003) 14806–14811. doi:10.1073/pnas.2036281100.

[9] J.-C. Leloup, A. Goldbeter, Toward a detailed computational model for the mammalian circadian clock, Proceedings of the National Academy of Sciences 100 (12) (2003) 7051 –7056. doi:10.1073/pnas.1132112100.

[10] S. Becker-Weimann, J. Wolf, H. Herzel, A. Kramer, Modeling feedback loops of the mammalian circadian oscillator, Biophysical Journal 87 (5) (2004) 3023–3034. doi:10.1529/biophysj.104.040824.

[11] T. O. Scheper, D. Klinkenberg, J. van Pelt, C. Pennartz, A model of molecular circadian clocks: multiple mechanisms for phase shifting and a requirement for strong nonlinear interactions, Journal of Biological Rhythms 14 (3) (1999) 213–220. doi:10.1177/074873099129000623.

[12] U. Abraham, A. E. Granada, P. O. Westermark, M. Heine, A. Kramer, H. Herzel, Coupling governs entrainment range of circadian clocks, Molecular Systems Biology 6 (1) (Jan. 2010). doi:10.1038/msb.2010.92.

[13] P. Ruoff, L. Rensing, The temperature-compensated Goodwin model simulates many circadian clock properties, Journal of Theoretical Biology 179 (4) (1996) 275–285. doi:10.1006/jtbi.1996.0067.

[14] J. J. Tyson, C. I. Hong, C. Dennis Thron, B. Novak, A simple model of circadian rhythms based on dimerization and proteolysis of PER and TIM, Biophysical Journal 77 (5) (1999) 2411–2417. doi:10.1016/S0006-3495(99)77078-5.

[15] H. P. Mirsky, A. C. Liu, D. K. Welsh, S. A. Kay, F. J. Doyle, A model of the cell-autonomous mammalian circadian clock, Proceedings of the National Academy of Sciences 106 (27) (2009) 11107 –11112. doi:10.1073/pnas.0904837106.

[16] A. Gundel, M. B. Spencer, A mathematical model of the human circadian system and its application to jet lag, Chronobiology International 9 (2) (1992) 148–159. doi:10.3109/07420529209064526.

[17] J.-C. Leloup, A. Goldbeter, Critical phase shifts slow down circadian clock recovery: Implications for jet lag, Journal of Theoretical Biology 333 (2013) 47–57. doi:10.1016/j.jtbi.2013.04.039.

[18] C. Bodenstein, M. Gosak, S. Schuster, M. Marhl, M. Perc, Modeling the seasonal adaptation of circadian clocks by changes in the network structure of the suprachiasmatic nucleus, PLoS Comput Biol 8 (9) (2012) e1002697. doi:10.1371/journal.pcbi.1002697.

[19] C. Schmal, J. Myung, H. Herzel, G. Bordyugov, A theoretical study on seasonality, Frontiers in Neurology 6 (May 2015). doi:10.3389/fneur.2015.00094.

[20] A. Pokhilko, S. K. Hodge, K. Stratford, K. Knox, K. D. Edwards, A. W. Thomson, T. Mizuno, A. J. Millar, Data assimilation constrains new connections and components in a complex, eukaryotic circadian clock model, Molecular Systems Biology 6 (1) (2010) 416. doi:10.1038/msb.2010.69.

[21] A. Relógio, P. O. Westermark, T. Wallach, K. Schellenberg, A. Kramer, H. Herzel, Tuning the mammalian circadian clock: Robust synergy of two loops, PLoS Comput Biol 7 (12) (2011) e1002309. doi:10.1371/journal.pcbi.1002309.

[22] A. Woller, H. Duez, B. Staels, M. Lefranc, A mathematical model of the liver circadian clock linking feeding and fasting cycles to clock function, Cell Reports 17 (4) (2016) 1087–1097. doi:10.1016/j.celrep.2016.09.060.

[23] C. S. Pittendrigh, Circadian systems: entrainment, in: J. Aschoff (Ed.), Biological Rhythms, Springer US, Boston, MA, 1981, pp. 95–124. doi:10.1007/978-1-4615-6552-9_7.

[24] C. H. Johnson, Phase Response Curves: What they tell us?, in: Circadian Clocks from Cell to Human, Hokkaido Univ. Press, Sapporo, 1992, pp. 209–246.

[25] A. Granada, R. Hennig, B. Ronacher, A. Kramer, H. Herzel, Chapter 1 Phase Response Curves, in: Methods in Enzymology, Vol. 454, Elsevier, 2009, pp. 1–27. doi:10.1016/S0076-6879(08)03801-9.

[26] S. B. S. Khalsa, M. E. Jewett, C. Cajochen, C. A. Czeisler, A phase response curve to single bright light pulses in human subjects, The Journal of Physiology 549 (3) (2003) 945–952. doi:10.1113/jphysiol.2003.040477.

[27] M. Comas, D. G. M. Beersma, K. Spoelstra, S. Daan, Phase and period responses of the circadian system of mice (mus musculus) to light stimuli of different duration, Journal of Biological Rhythms 21 (5) (2006) 362–372. doi:10.1177/0748730406292446.

[28] D. F. Kripke, J. A. Elliott, S. D. Youngstedt, K. M. Rex, Circadian phase response curves to light in older and young women and men, Journal of Circadian Rhythms 5 (0) (2007) 4. doi:10.1186/1740-3391-5-4.

[29] S. Kiessling, G. Eichele, H. Oster, Adrenal glucocorticoids have a key role in circadian resynchronization in a mouse model of jet lag, Journal of Clinical Investigation 120 (7) (2010) 2600–2609. doi:10.1172/JCI41192.

[30] A. E. Granada, G. Bordyugov, A. Kramer, H. Herzel, Human chronotypes from a theoretical perspective, PLoS ONE 8 (3) (Mar. 2013). doi:10.1371/journal.pone.0059464.

[31] A. T. Winfree, Integrated view of resetting a circadian clock, Journal of Theoretical Biology 28 (3) (1970) 327–374. doi:10.1016/0022-5193(70)90075-5.

[32] S. Yamazaki, Resetting central and peripheral circadian oscillators in transgenic rats, Science 288 (5466) (2000) 682–685. doi:10.1126/science.288.5466.682.

[33] A. B. Reddy, M. D. Field, E. S. Maywood, M. H. Hastings, Differential resynchronisation of circadian clock gene expression within the suprachiasmatic nuclei of mice subjected to experimental jet lag, The Journal of Neuroscience 22 (17) (2002) 7326–7330. doi:10.1523/JNEUROSCI.22-17-07326.2002.

[34] M. J. Vansteensel, S. Yamazaki, H. Albus, T. Deboer, G. D. Block, J. H. Meijer, Dissociation between circadian Per1 and neuronal and behavioral rhythms following a shifted environmental cycle, Current Biology 13 (17) (2003) 1538–1542. doi:10.1016/S0960-9822(03)00560-8.

[35] J. C. Locke, P. O. Westermark, A. Kramer, H. Herzel, Global parameter search reveals design principles of the mammalian circadian clock, BMC Systems Biology 2 (1) (2008) 22. doi:10.1186/1752-0509-2-22.

[36] S. Daan, J. Aschoff, Circadian rhythms of locomotor activity in captive birds and mammals: Their variations with season and latitude, Oecologia 18 (4) (1975) 269–316. doi:10.1007/BF00345851.

[37] J. Rémi, M. Merrow, T. Roenneberg, A circadian surface of entrainment: varying t, τ, and photoperiod in *neurospora crassa*, Journal of Biological Rhythms 25 (5) (2010) 318–328. doi:10.1177/0748730410379081.

[38] C. S. Pittendrigh, S. Daan, A functional analysis of circadian pacemakers in nocturnal rodents, Journal of comparative physiology 106 (3) (1976) 291–331. doi:10.1007/BF01417859.

[39] B. Ananthasubramaniam, H. Herzel, Positive feedback promotes oscillations in negative feedback loops, PLoS ONE 9 (8) (2014) e104761. doi:10.1371/journal.pone.0104761.

[40] K. P. Wright, C. Gronfier, J. F. Duffy, C. A. Czeisler, Intrinsic period and light intensity determine the phase relationship between melatonin and sleep in humans, Journal of Biological Rhythms 20 (2) (2005) 168–177. doi:10.1177/0748730404274265.

[41] R. A. Wever, The circadian system of man: results of experiments under temporal isolation, Topics in environmental physiology and medicine, Springer-Verlag, New York, 1979.

[42] J. Aschoff, H. Pohl, Phase relations between a circadian rhythm and its zeitgeber within the range of entrainment, Naturwissenschaften 65 (2) (1978) 80–84. doi:10.1007/BF00440545.

[43] G. Kurosawa, A. Goldbeter, Amplitude of circadian oscillations entrained by 24-h light–dark cycles, Journal of Theoretical Biology 242 (2) (2006) 478–488. doi:10.1016/j.jtbi.2006.03.016.

[44] A. E. Granada, H. Herzel, How to achieve fast entrainment? The timescale to synchronization, PLoS ONE 4 (9) (2009) e7057. doi:10.1371/journal.pone.0007057.

[45] J. Griffith, Mathematics of cellular control processes I. Negative feedback to one gene, Journal of Theoretical Biology 20 (2) (1968) 202–208. doi:10.1016/0022-5193(68)90189-6.

[46] J. Myung, C. Schmal, S. Hong, Y. Tsukizawa, P. Rose, Y. Zhang, M. J. Holtzman, E. De Schutter, H. Herzel, G. Bordyugov, T. Takumi, The choroid plexus is an important circadian clock component, Nature Communications 9 (1) (2018) 1062. doi:10.1038/s41467-018-03507-2.

[47] M. H. Vitaterna, C. H. Ko, A.-M. Chang, E. D. Buhr, E. M. Fruechte, A. Schook, M. P. Antoch, F. W. Turek, J. S. Takahashi, The mouse Clock mutation reduces circadian pacemaker amplitude and enhances efficacy of resetting stimuli and phase-response curve amplitude, Proceedings of the National Academy of Sciences 103 (24) (2006) 9327–9332. doi:10.1073/pnas.0603601103.

[48] H. Ukai, T. J. Kobayashi, M. Nagano, K.-h. Masumoto, M. Sujino, T. Kondo, K. Yagita, Y. Shigeyoshi, H. R. Ueda, Melanopsin-dependent photo-perturbation reveals desynchronization underlying the singularity of mammalian circadian clocks, Nature Cell Biology 9 (11) (2007) 1327–1334. doi:10.1038/ncb1653.

[49] Y. Yamaguchi, T. Suzuki, Y. Mizoro, H. Kori, K. Okada, Y. Chen, J.-M. Fustin, F. Yamazaki, N. Mizuguchi, J. Zhang, X. Dong, G. Tsujimoto, Y. Okuno, M. Doi, H. Okamura, Mice genetically deficient in vasopressin V1a and V1b receptors are resistant to jet lag, Science 342 (6154) (2013) 85–90. doi:10.1126/science.1238599.

[50] S. An, R. Harang, K. Meeker, D. Granados-Fuentes, C. A. Tsai, C. Mazuski, J. Kim, F. J. Doyle, L. R. Petzold, E. D. Herzog, A neuropeptide speeds circadian entrainment by reducing intercellular synchrony, Proceedings of the National Academy of Sciences 110 (46) (2013) E4355–E4361. doi:10.1073/pnas.1307088110.

[51] D. Gonze, S. Bernard, C. Waltermann, A. Kramer, H. Herzel, Spontaneous synchronization of coupled circadian oscillators, Biophysical Journal 89 (1) (2005) 120–129. doi:10.1529/biophysj.104.058388.

[52] A. Korenčič, G. Bordyugov, R. Košir, D. Rozman, M. Goličnik, H. Herzel, The interplay of cis-regulatory elements rules circadian rhythms in mouse liver, PLoS ONE 7 (11) (2012) e46835. doi:10.1371/journal.pone.0046835.

[53] J. P. Pett, M. Kondoff, G. Bordyugov, A. Kramer, H. Herzel, Co-existing feedback loops generate tissue-specific circadian rhythms, Life Science Alliance 1 (3) (2018) e201800078. doi:10.26508/lsa.201800078.

[54] J. S. Takahashi, Transcriptional architecture of the mammalian circadian clock, Nature Reviews Genetics 18 (3) (2017) 164–179. doi:10.1038/nrg.2016.150.

[55] E. E. Zhang, A. C. Liu, T. Hirota, L. J. Miraglia, G. Welch, P. Y. Pongsawakul, X. Liu, A. Atwood, J. W. Huss, J. Janes, A. I. Su, J. B. Hogenesch, S. A. Kay, A Genome-wide RNAi Screen for Modifiers of the Circadian Clock in Human Cells, Cell 139 (1) (2009) 199–210. doi:10.1016/j.cell.2009.08.031.

[56] D. Mauvoisin, J. Wang, C. Jouffe, E. Martin, F. Atger, P. Waridel, M. Quadroni, F. Gachon, F. Naef, Circadian clock-dependent and -independent rhythmic proteomes implement distinct diurnal functions in mouse liver, Proceedings of the National Academy of Sciences 111 (1) (2014) 167–172. doi:10.1073/pnas.1314066111.

[57] R. Zhang, N. F. Lahens, H. I. Ballance, M. E. Hughes, J. B. Hogenesch, A circadian gene expression atlas in mammals: Implications for biology and medicine, Proceedings of the National Academy of Sciences 111 (45) (2014) 16219–16224. doi:10.1073/pnas.1408886111.

[58] R. E. Kronauer, D. B. Forger, M. E. Jewett, Quantifying human circadian pacemaker response to brief, extended, and repeated light stimuli over the phototopic range, Journal of Biological Rhythms 14 (6) (1999) 501–516. doi:10.1177/074873049901400609.

[59] B. Ananthasubramaniam, E. D. Herzog, H. Herzel, Timing of neuropeptide coupling determines synchrony and entrainment in the mammalian circadian clock, PLoS Comput Biol 10 (4) (2014) e1003565. doi:10.1371/journal.pcbi.1003565.

[60] J. K. Kim, D. B. Forger, A mechanism for robust circadian timekeeping via stoichiometric balance, Molecular Systems Biology 8 (1) (Dec. 2012). doi:10.1038/msb.2012.62.

[61] B. C. Goodwin, Oscillatory behavior in enzymatic control processes, Advances in Enzyme Regulation 3 (1965) 425–437. doi:10.1016/0065-2571(65)90067-1.

[62] M. C. Mackey, Periodic auto-immune hemolytic anemia: An induced dynamical disease, Bulletin of Mathematical Biology 41 (6) (1979) 829–834. doi:10.1007/BF02462379.

[63] N. MacDonald, Biological delay systems: linear stability theory, digitally print. version with corrections Edition, no. 9 in Cambridge studies in mathematical biology, Cambridge University Press, Cambridge, 2008, oCLC: 780134302.

[64] R. Lev Bar-Or, R. Maya, L. A. Segel, U. Alon, A. J. Levine, M. Oren, Generation of oscillations by the p53-Mdm2 feedback loop: A theoretical and experimental study, Proceedings of the National Academy of Sciences 97 (21) (2000) 11250–11255. doi:10.1073/pnas.210171597.

[65] Y. Bessho, R. Kageyama, Oscillations, clocks and segmentation, Current Opinion in Genetics & Development 13 (4) (2003) 379–384. doi:10.1016/S0959-437X(03)00083-2.

[66] R. Cheong, A. Hoffmann, A. Levchenko, Understanding NF-κB signaling via mathematical modeling, Molecular Systems Biology 4 (1) (2008) 192. doi:10.1038/msb.2008.30.

[67] P. Meyer, PER-TIM interactions in living drosophila cells: An interval timer for the circadian clock, Science 311 (5758) (2006) 226–229. doi:10.1126/science.1118126.

[68] N. Y. Garceau, Y. Liu, J. J. Loros, J. C. Dunlap, Alternative initiation of translation and time-specific phosphorylation yield multiple forms of the essential clock protein FREQUENCY, Cell 89 (3) (1997) 469–476. doi:10.1016/S0092-8674(00)80227-5.

[69] K. Vanselow, J. T. Vanselow, P. O. Westermark, S. Reischl, B. Maier, T. Korte, A. Herrmann, H. Herzel, A. Schlosser, A. Kramer, Differential effects of PER2 phosphorylation: molecular basis for the human familial advanced sleep phase syndrome (FASPS), Genes & Development 20 (19) (2006) 2660–2672. doi:10.1101/gad.397006.

[70] C. Querfurth, A. Diernfellner, F. Heise, L. Lauinger, A. Neiss, O. Tataroglu, M. Brunner, T. Schafmeier, Posttranslational regulation of *Neurospora* circadian clock by ck1a-dependent phosphorylation, Cold Spring Harbor Symposia on Quantitative Biology 72 (1) (2007) 177–183. doi:10.1101/sqb.2007.72.025.

[71] Y. Isojima, M. Nakajima, H. Ukai, H. Fujishima, R. G. Yamada, K.-h. Masumoto, R. Kiuchi, M. Ishida, M. Ukai-Tadenuma, Y. Minami, R. Kito, K. Nakao, W. Kishimoto, S.-H. Yoo, K. Shimomura, T. Takao, A. Takano, T. Kojima, K. Nagai, Y. Sakaki, J. S. Takahashi, H. R. Ueda, CKIϵ/δ-dependent phosphorylation is a temperature-insensitive, period-determining process in the mammalian circadian clock, Proceedings of the National Academy of Sciences 106 (37) (2009) 15744–15749. doi:10.1073/pnas.0908733106.

[72] R. P. Aryal, P. B. Kwak, A. G. Tamayo, M. Gebert, P.-L. Chiu, T. Walz, C. J. Weitz, Macromolecular assemblies of the mammalian circadian clock, Molecular Cell 67 (5) (2017) 770–782.e6. doi:10.1016/j.molcel.2017.07.017.

[73] N. Koike, S.-H. Yoo, H.-C. Huang, V. Kumar, C. Lee, T.-K. Kim, J. S. Takahashi, Transcriptional architecture and chromatin landscape of the core circadian clock in mammals, Science 338 (6105) (2012) 349–354. doi:10.1126/science.1226339.

[74] C. Thron, The secant condition for instability in biochemical feedback control—I. The role of cooperativity and saturability, Bulletin of Mathematical Biology 53 (3) (1991) 383–401. doi:10.1016/S0092-8240(05)80394-5.

[75] J. K. Kim, Protein sequestration versus Hill-type repression in circadian clock models, IET Systems Biology 10 (4) (2016) 125–135. doi:10.1049/iet-syb.2015.0090.

[76] A. Upadhyay, M. Brunner, H. Herzel, An Inactivation Switch Enables Rhythms in a Neurospora Clock Model, International Journal of Molecular Sciences 20 (12) (2019) 2985. doi:10.3390/ijms20122985.

[77] J. E. Ferrell, S. H. Ha, Ultrasensitivity part I: Michaelian responses and zero-order ultrasensitivity, Trends in Biochemical Sciences 39 (10) (2014) 496–503. doi:10.1016/j.tibs.2014.08.003.

[78] A. L. Hodgkin, A. F. Huxley, A quantitative description of membrane current and its application to conduction and excitation in nerve, The Journal of Physiology 117 (4) (1952) 500–544. doi:10.1113/jphysiol.1952.sp004764.

[79] J. J. Tyson, K. C. Chen, B. Novak, Sniffers, buzzers, toggles and blinkers: dynamics of regulatory and signaling pathways in the cell, Current Opinion in Cell Biology 15 (2) (2003) 221–231. doi:10.1016/S0955-0674(03)00017-6.

[80] A. Goldbeter, D. E. Koshland, An amplified sensitivity arising from covalent modification in biological systems., Proceedings of the National Academy of Sciences of the United States of America 78 (11) (1981) 6840–6844.

[81] S. Legewie, N. Blüthgen, H. Herzel, Mathematical modeling identifies inhibitors of apoptosis as mediators of positive feedback and bistability, PLoS Computational Biology 2 (9) (2006) e120. doi:10.1371/journal.pcbi.0020120.

[82] M. Zhou, J. Kim, G. Eng, D. Forger, D. Virshup, A period2 phosphoswitch regulates and temperature compensates circadian period, Molecular Cell 60 (1) (2015) 77–88. doi:10.1016/j.molcel.2015.08.022.

[83] M. J. Emmett, M. A. Lazar, Integrative regulation of physiology by histone deacetylase 3, Nature Reviews Molecular Cell Biology 20 (2) (2019) 102–115. doi:10.1038/s41580-018-0076-0.

[84] X. Liu, Y. Dang, T. Matsu-ura, Y. He, Q. He, C. I. Hong, Y. Liu, DNA replication is required for circadian clock function by regulating rhythmic nucleosome composition, Molecular Cell 67 (2) (2017) 203–213.e4. doi:10.1016/j.molcel.2017.05.029.

[85] A. Erzberger, G. Hampp, A. E. Granada, U. Albrecht, H. Herzel, Genetic redundancy strengthens the circadian clock leading to a narrow entrainment range, Journal of The Royal Society Interface 10 (84) (2013) 20130221. doi:10.1098/rsif.2013.0221.

[86] M. Merrow, M. Brunner, T. Roenneberg, Assignment of circadian function for the Neurospora clock gene frequency, Nature 399 (6736) (1999) 584–586. doi:10.1038/21190.

[87] P. L. Lakin-Thomas, S. Brody, G. G. Coté, Amplitude model for the effects of mutations and temperature on period and phase resetting of the Neurospora circadian oscillator, Journal of Biological Rhythms 6 (4) (1991) 281–297. doi:10.1177/074873049100600401.

[88] B. Wang, A. N. Kettenbach, X. Zhou, J. J. Loros, J. C. Dunlap, The phospho-code determining circadian feedback loop closure and output in Neurospora, Molecular Cell 74 (4) (2019) 771–784.e3. doi:10.1016/j.molcel.2019.03.003.

[89] S. R. Pulivarthy, N. Tanaka, D. K. Welsh, L. De Haro, I. M. Verma, S. Panda, Reciprocity between phase shifts and amplitude changes in the mammalian circadian clock, Proceedings of the National Academy of Sciences 104 (51) (2007) 20356–20361. doi:10.1073/pnas.0708877104.

[90] S. A. Brown, D. Kunz, A. Dumas, P. O. Westermark, K. Vanselow, A. Tilmann-Wahnschaffe, H. Herzel, A. Kramer, Molecular insights into human daily behavior, Proceedings of the National Academy of Sciences 105 (5) (2008) 1602–1607. doi:10.1073/pnas.0707772105.

[91] R. K. Barrett, J. S. Takahashi, Lability of circadian pacemaker amplitude in chick pineal cells: a temperature-dependent process, Journal of Biological Rhythms 12 (4) (1997) 309–318. doi:10.1177/074873049701200403.

[92] C. S. Pittendrigh, W. T. Kyner, T. Takamura, The amplitude of circadian oscillations: temperature dependence, latitudinal clines, and the photoperiodic time measurement, Journal of Biological Rhythms 6 (4) (1991) 299–313. doi:10.1177/074873049100600402.

[93] G. Kurosawa, A. Mochizuki, Y. Iwasa, Comparative study of circadian clock models, in search of processes promoting oscillation, Journal of Theoretical Biology 216 (2) (2002) 193–208. doi:10.1006/jtbi.2002.2546.

[94] E. J. Doedel, T. F. Fairgrieve, B. Sandstede, A. R. Champneys, Y. A. Kuznetsov, X. Wang, AUTO-07p: Continuation and bifurcation software for ordinary differential equations, Tech. rep. (2007).

[95] C. Schmal, J.-C. Leloup, D. Gonze, Modeling and simulating the *Arabidopsis thaliana* circadian clock using XPP-AUTO, in: D. Staiger (Ed.), Plant Circadian Networks, Vol. 1158, Springer New York, New York, NY, 2014, pp. 337–358. doi:10.1007/978-1-4939-0700-7_23.

8. Supplementary Figures

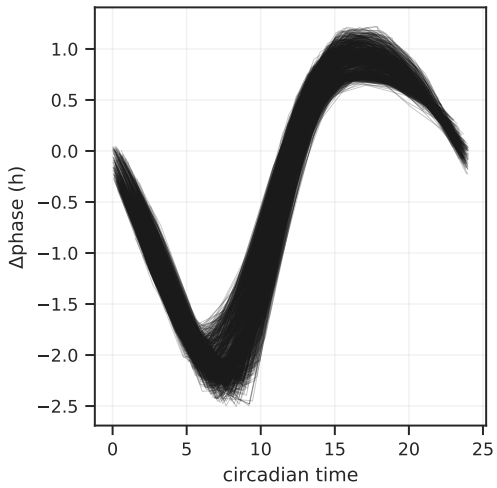

Figure S1: Phase response curves (PRCs) for the set of models. The PRC to a one hour pulse for all models in the ensemble with the pulse time scaled by the intrinsic clock period in order to make the PRCs comparable.

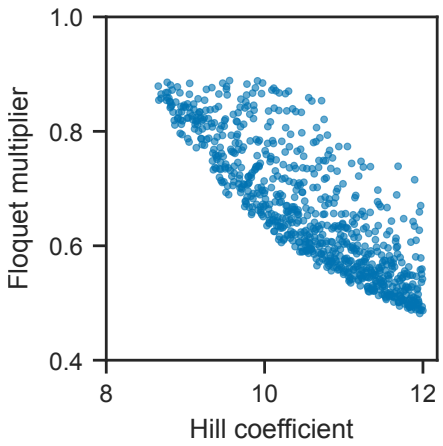

Figure S2: Floquet multiplier of the Goodwin model for different Hill coefficients. The amplitude relaxation rate is $-\log(\text{Floquet multiplier})$.

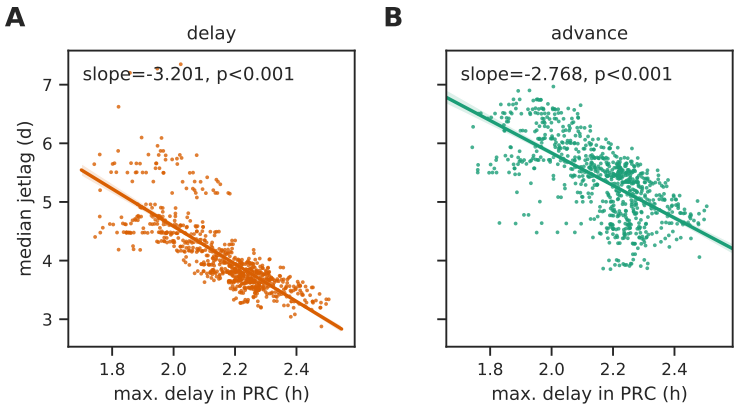

Figure S3: Jetlag duration for models with different PRCs. (A) The dependence of duration of 6h delay jetlag on the features of the PRC to a one hour pulse, i.e., the maximum maximum delay shifts in the PRC. (B) The dependence of the duration of a 6h advance jetlag on the maximum delay shifts in the PRC. The dependence on maximum advance of (A) and (B) is just the mirror image, since by design the sum of maximum advance and maximum delay is approximately three hours. The p-value for the slope obtained from linear regression is shown for all plots.

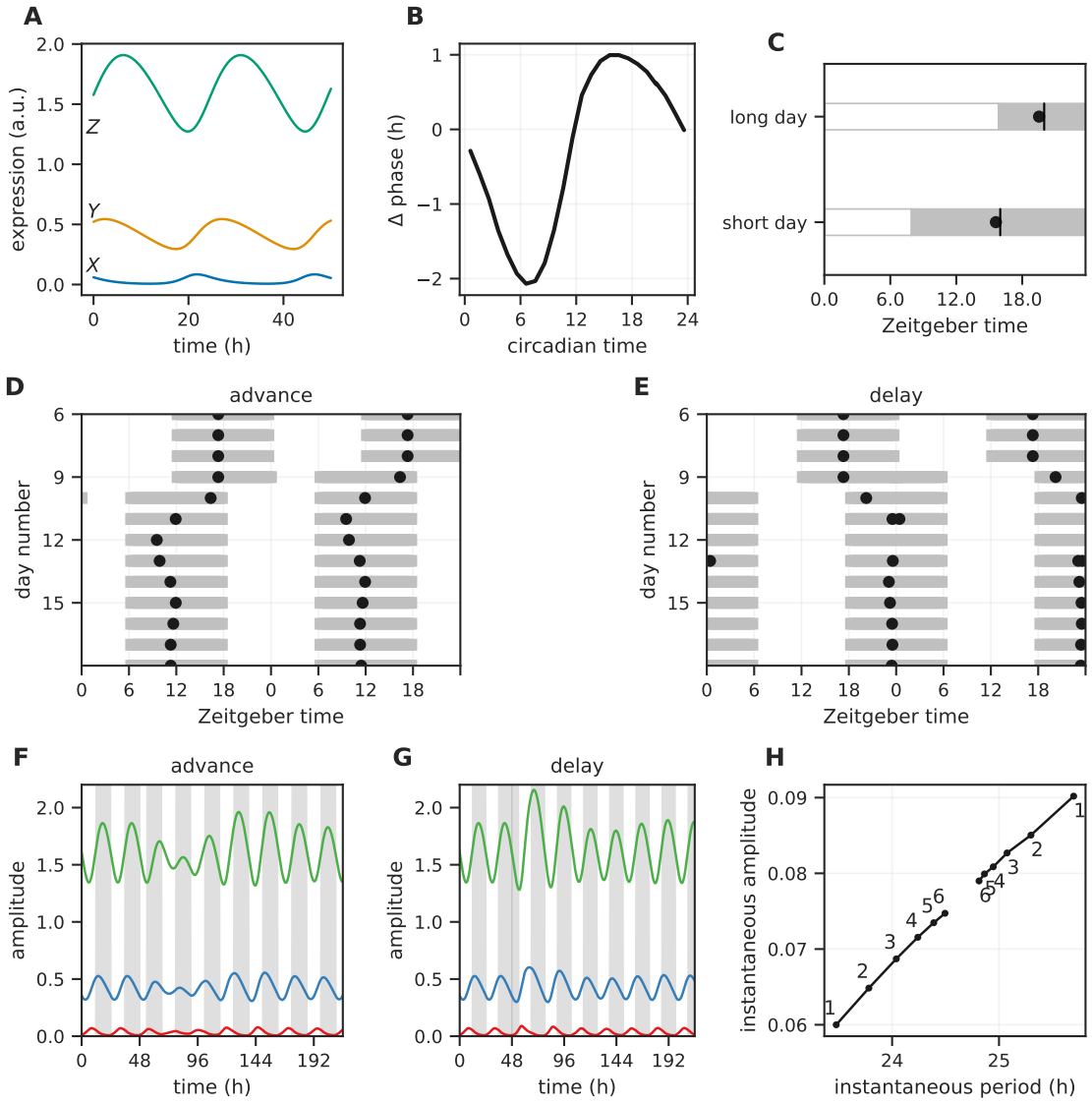

Figure S4: Representative model with positive feedback in the ensemble (compare with Figures 2 and 6). (A) Time series of the three states of a representative model with positive feedback (Figure 1C). The time series corresponding to each model variable is marked. (B) The phase response curve for the model in (A) in response to a one-hour pulse. (C) The phase of entrainment (black dots) measured relative to lights on under long day (16h light, 8h dark) and short day (8h light, 16h dark). The phase of entrainment is acrophase of variable Z. (D, E) The acrophase of variable Z (black dot) during a 6h simulated jetlag from Berlin to New York (delay) or New York to Berlin (advance). (F,G) Time series of the model during a 6h jetlag advance (F) and a 6h jetlag delay (G). The dark period of the light-dark cycle is colored grey. Jetlag occurs at $t \sim 49$h. (H) A measure of the twist (amplitude-period association) of the representative model. The instantaneous amplitude and period of the model as it returns to the unperturbed state after a perturbation of $\epsilon = 0.1$ in a random direction. Amplitude of variable X is used as the amplitude measure. Model Parameters: $d_1 = 0.29\text{h}^{-1}, d_2 = 0.20\text{h}^{-1}, d_3 = 0.26\text{h}^{-1}, K = 0.92, h = 10.01, \tau = 24.71\text{h}$.

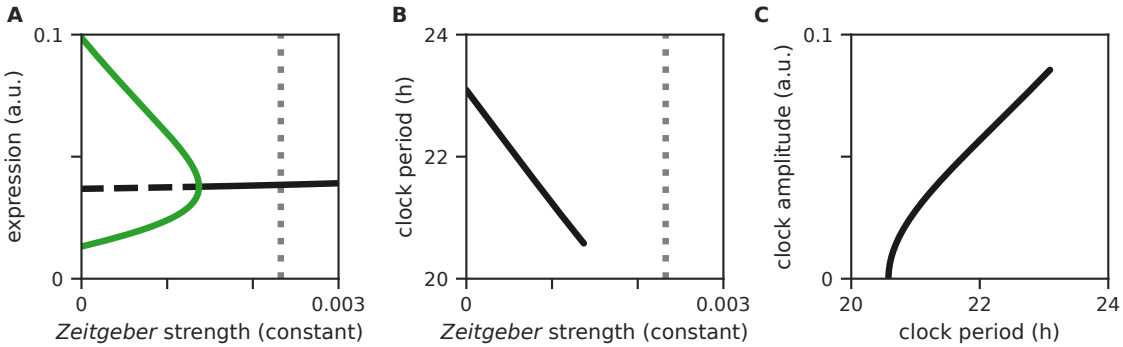

Figure S5: Bifurcation analysis of the representative model from Figure 2. (A) The behavior of the model for different levels of constant *Zeitgeber* input. The stable steady-states are denoted by solid black lines and unstable steady-states by dashed black lines. The green line represents the maximum and minimum expression levels of the Z variable in the limit cycle regime. To the right of this region, only damped oscillations ensue. (B) The period of the model within the limit cycle regime in (A). (C) The amplitude-period covariation of the model within the limit cycle regime in (A). The grey dotted line is the *Zeitgeber* strength used for this model in Figure 8.